Fast-ion D_α measurements and simulations in quiet plasmas

Y. Luo and W. W. Heidbrink
University of California, Irvine, California 92697, USA

K. H. Burrell
General Atomics, P.O. Box 85608, San Diego, California 92186, USA

E. Ruskov
University of California, Irvine, California 92697, USA

W. M. Solomon
Princeton Plasma Physics Laboratory, Princeton University, Princeton, New Jersey 08543, USA

(Received 11 June 2007; accepted 13 September 2007; published online 7 November 2007)

The D_α light emitted by neutralized deuterium fast ions is measured in magnetohydrodynamics (MHD)-quiescent, magnetically confined plasmas during neutral beam injection. A weighted Monte Carlo simulation code models the fast-ion D_α spectra based on the fast-ion distribution function calculated classically by TRANSP [R. V. Budny, Nucl. Fusion **34**, 1247 (1994)]. The spectral shape is in excellent agreement and the magnitude also has reasonable agreement. The fast-ion D_α signal has the expected dependencies on various parameters including injection energy, injection angle, viewing angle, beam power, electron temperature, and electron density. The neutral particle diagnostic and measured neutron rate corroborate the fast-ion D_α measurements. The relative spatial profile agrees with TRANSP and is corroborated by the fast-ion pressure profile inferred from the equilibrium. © *2007 American Institute of Physics*. [DOI: 10.1063/1.2794320]

I. INTRODUCTION

In tokamaks, fast ions are generated by injection of neutral beams, by rf acceleration, and by fusion reactions. They can be a major source of energy, momentum, and particles for the plasma. In ITER,[1] energetic alpha particles produced from fusion reactions are required to sustain ignition of the plasma. However, alpha particles may drive Alfvén eigenmodes unstable, which could result in anomalous fast-ion transport.[2,3] To study this important issue, detailed measurements of fast-ion spatial profiles are essential. Although several diagnostic techniques exist, fast-ion D_α (FIDA) spectroscopy[4] has good spatial, energy, and temporal resolution[5] and nicely complements established techniques.[6]

FIDA measures the D_α spectrum produced by neutralized fast ions (reneutrals) born in charge-exchange events with injected neutrals and halo neutrals. It is a type of charge-exchange spectroscopy similar to the technique used to measure alpha particles in the Tokamak Fusion Test Reactor[7] and accelerated helium ions in the Joint European Torus.[8] In real space, FIDA is a localized measurement with the observational volume defined primarily by the intersection of the viewing line with the neutral beam. In velocity space, it is a one-dimensional measurement with similarities to collective Thomson scattering.[9] Therefore, a collection of fast ions in pitch and energy space can contribute to each specific wavelength. A dedicated FIDA diagnostic was developed in DIII-D in the 2005 campaign.[10] Before utilizing this instrument to study fast-ion transport by collective instabilities, a thorough benchmark is required to validate this novel diagnostic technique. MHD-quiescent plasmas provide an ideal testbed for this purpose since fast ions decelerate classically and hardly diffuse in such quiet plasmas with dilute fast-ion populations.[2] As shown in this paper, the excellent agreement between the data and classical predictions in these quiet plasmas validates the FIDA technique.

The article is organized as follows. Section II describes the apparatus, plasma conditions, other fast-ion diagnostics, and the FIDA database. Section III introduces the simulation code and compares the measurements with the prediction. FIDA dependencies on a variety of parameters are shown and corroboration by other fast-ion diagnostics is presented (Sec. IV). Section V shows FIDA spatial profiles. The conclusion is in Sec. VI. In the Appendix, the sensitivity of the simulated spectrum on various input parameters is investigated.

II. EXPERIMENTAL SETUP

The measurements are from DIII-D, a moderate-sized tokamak (major radius $R_0 \approx 1.7$ m, minor radius $a \approx 0.6$ m). The primary source of auxiliary heating for the plasma is seven neutral beams, which usually inject 71–80 keV deuterium neutrals in the direction of the plasma current into deuterium plasmas at two angles with respect to the toroidal field. For neutrals injected by the more perpendicular "right" beams, the tangency radius is $R_{\tan} \approx 0.76$ m; for the more tangential "left" beams, $R_{\tan} \approx 1.15$ m. Another source of auxiliary heating is electron cyclotron heating (ECH), which transfers energy to electrons at the second cyclotron harmonic resonance. A common technique to control electron temperature is to modulate the ECH. Typical electron density, carbon density, electron temperature, and ion temperature profiles are shown in Fig. 1. The electron density is measured by Thomson scattering[11] corroborated by CO_2 interferometry.[12] Thomson scattering and electron cyclotron

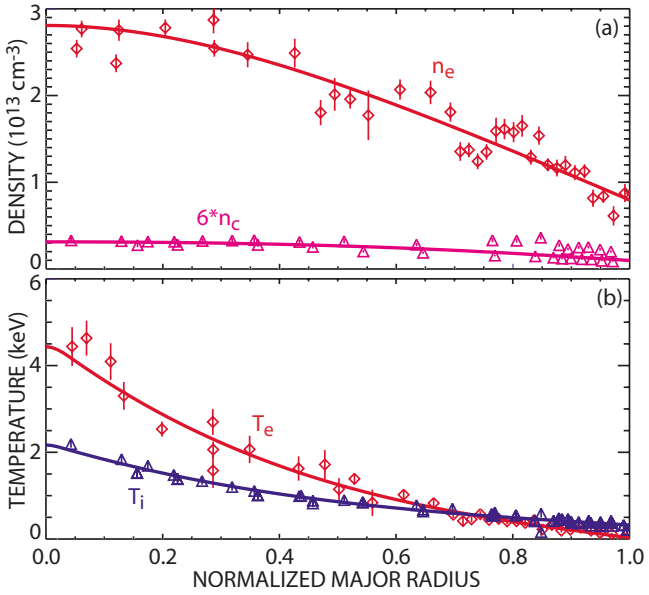

FIG. 1. (Color online) Profiles of (a) electron density, carbon density (×6), (b) electron temperature, and ion temperature in discharge 122985 at 1365 ms.

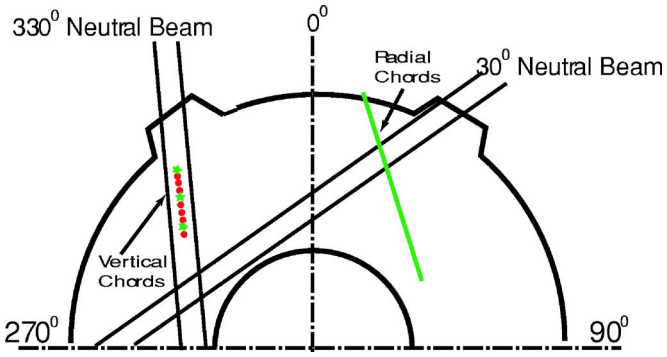

FIG. 2. (Color online) FIDA fiber views shown on the midplane. The fiber views for the dedicated system are shown in stars, and those for the Reticon system in dots. The detector of the radial chord is located at the midplane, while the detector of the vertical chords is located at a port under the midplane. Only left beams (R_{tan}=1.15 m) are shown in the figure.

emission[13] measure the electron temperature. The data presented in this paper are from quiet, L-mode plasmas. MHD activity and Alfvén activity are minimal in the discharges. There are no detectable kinks or tearing modes on the magnetic signals and the fishbones and sawteeth are small. Coherent Alfvén activity between 50 and 300 kHz is undetectable on the magnetics and on a sensitive, low-k, far-infrared scattering[14] diagnostic.

There are two pre-existing fast-ion diagnostics installed on DIII-D, neutron detectors[15] and a neutral particle analyzer.[16] Neutron scintillator measures neutrons generated by fusion reactions. Under these conditions, beam-thermal reactions dominate the total neutron rate. Neutron scintillator is a volume-integrated diagnostic both in real space and in velocity space. The neutral particle analyzer directly measures fast ions neutralized by charge-exchange reactions. Like FIDA, it is a localized diagnostic since it is an active charge-exchange diagnostic. In contrast to FIDA, it only detects fast ions moving toward the detector along the vertical viewing line.

For the data in this paper, the FIDA diagnostic consists of two separate systems, a dedicated CCD-based system and a photodiode-based Reticon system, usually used for charge-exchange recombination spectroscopy. The dedicated system measures the entire spectrum and has a better signal-to-noise ratio (SNR) since it is equipped with a high quantum efficiency CCD as the detector. It can take two spectra simultaneously with the capability of switching fibers between discharges. The Reticon system measures a portion of the spectrum, usually the blue side, which has fewer impurity contaminants.[5] A common technique to improve the SNR of the Reticon measurements is to average over a large time window during steady plasma conditions. Figure 2 shows the fiber views for the data analyzed in this paper. For all of the vertical views, the collection lens is located at a port under the midplane. Although the chords are designed to view the left beam with 1.15 m tangency radius, some of them do see a small portion of the right beam with 0.76 m tangency radius, especially the outer chords.

The raw FIDA data are a two-dimensional array in pixels and time. Each pixel corresponds to a specific wavelength (λ), which translates into a velocity or energy (E_λ) through the Doppler shift formula,

$$\lambda = \lambda_0(1 - v/c), \tag{1}$$

where λ_0 is the rest D_α wavelength, c is the speed of light in vacuum, and v is the velocity component along the viewing line. v is positive when the reneutrals move toward the detector. E_λ is the energy component of the reneutral along the viewing line, instead of the total energy. The standard procedure[5] of analyzing the FIDA data is as follows. First, unusable time slices are removed, for instance, those contaminated by edge localized modes. Second, contaminated pixels by neutron/gamma hits are replaced with an average of the neighboring pixels. After the above initial processing, background subtraction is essential to remove contaminants such as scattered light, visible bremsstrahlung, non-charge-exchange impurity lines, etc. In quiet plasmas, we usually do background subtraction via beam modulation. A certain time window during which the plasma is steady is selected first. Beam-on and beam-off spectra are then averaged over the time window. The averaged beam-off spectrum is subtracted from the averaged beam-on spectrum next. The resultant spectrum has two impurity lines excited by charge exchange and the halo line, which are removed by fitting. The final spectrum is the pure FIDA spectrum that can be analyzed in various ways. A common practice is to average over a certain E_λ window to quantify the FIDA signal strength using a single number. The FIDA signal is proportional to the fast-ion density, the neutral density, and the averaged reaction rate because of the charge-exchange reaction. The averaged reaction rate depends on the fast-ion velocity distribution function, which is determined by Coulomb collisions in quiet plasmas without rf heating. In such plasma conditions, the averaged reaction rate is insensitive to plasma conditions and can be assumed to be a constant. To generate a quantity that

is proportional to the fast-ion density, we often divide the FIDA signal by the neutral density. We call this quantity FIDA density. The error bar associated with random errors can be estimated assuming the spectra are stationary in the selected time window. The standard deviations of the averaged beam-on signal and beam-off signal are calculated first based on the ensemble of the beam-on and beam-off time slices. The error bar is the square root of the sum of squares of the standard deviations.

To study parametric dependencies and correlations of the FIDA signal, a database with around 700 entries of plasmas with steady conditions for over 200 ms is built from the 2005 campaign. Each entry corresponds to a discharge and an averaging time window which is typically 200 ms. For each entry, there is a substantial amount of information saved. A partial list relevant to this paper includes the following: plasma parameters (electron density, electron temperature), beam parameters (total power, left beam fraction, beam modulation pattern), ion cyclotron heating (ICH) power, instability flag [magnetohydrodynamics (MHD), toroidal Alfvén eigenmode (AE)], neutron rate, neutral particle analyzer (NPA) signal, and FIDA signal.

III. SPECTRAL SHAPE AND MAGNITUDE

A. Simulation code

The FIDA diagnostic is a one-dimensional measurement in velocity space. It is theoretically impossible to convert the FIDA spectrum to a fast-ion distribution function.[17] Nevertheless, for a specific fast-ion distribution function, the FIDA spectrum can be predicted. The FIDA spectral shape is distorted with respect to the one-dimensional velocity space shape by various atomic rates, especially the charge-exchange rate between fast ions and neutrals. Moreover, for each specific wavelength Doppler shift, a collection of fast ions with different energies and pitch angles contributes to the spectral intensity. The weighting in velocity space is complicated.[5] The complex nature of the problem of converting a fast-ion distribution to the FIDA spectrum makes simulation the only solution.

A Cartesian grid is employed for the weighted Monte Carlo (MC) simulation code[4] to facilitate the calculation of the trajectory of reneutrals. The code begins with a steady calculation of the beam and halo neutral distributions with energy level (n) tracked through 1 to 4 and mapping of magnetic and electric fields, plasma parameters, and the fast-ion distribution function into each "cell." Based on the neutral distribution and the fast-ion density in each cell, the number of reneutrals is determined to launch in each cell. The initial velocity of each reneutral is found using a Monte Carlo rejection test in the two dimensions that describe the velocity distribution (energy and pitch). With the velocity now specified, the actual reaction rate of the fast ion with the neutrals can be computed and it is assigned to be the weight of the reneutral. Each reneutral actually represents a family of reneutrals with energy level 1 to 4 and the same velocity. The probability of each energy level is calculated based on the neutral density and charge-exchange rates. The trajectory of the reneutral through the cells is calculated next. As the reneutral travels through each cell, the time-dependent collisional-radiative balance between states is computed, including the number of D_α photons that are emitted. The Stark effect and Doppler shifts of emitted photons, given the local electric and magnetic fields and the velocities of the reneutral, are calculated. Finally, the spectrum is integrated over the observation volume for each viewing chord.

The running time of the simulation code is proportional to the number of reneutrals launched and roughly scales as $\sqrt[3]{n_g}$, in which n_g is the total number of grid cells. The multiple-dimensional nature of the fast-ion distribution function requires a large number of reneutrals (usually 10^7) to be launched. n_g is determined by the volume of region of interest and the grid size. The largest grid size can be set around the diagnostic resolution, which is ~4 cm. The most time consuming part of the code is to form and solve the collisional-radiative differential equations. Most of the coefficients of the differential equations are the reaction rates of reneutrals with thermal ions, electrons, and impurities, which are primarily carbons. In general, reactivity $\langle \sigma v \rangle$ for collisions depends on the relative velocity. To simplify, we assume that $v_e \gg v_f \gg v_c$, where v_e is electron velocity, v_f is fast-ion velocity, and v_c is carbon velocity. Therefore, for electron collisions with reneutrals, the reaction rate is merely a function of electron temperature, and for carbon collisions with reneutrals, the reaction rate is merely a function of reneutral velocity.

B. Comparison

The simulation output is the number of photons detected by the collection lens, while the measurement is the number of digitizer counts from the CCD camera. To do absolute comparison between the simulation and the measurement, an intensity calibration is performed to convert photons on the collection lens to digitizer counts from the CCD camera for each channel.

Figure 3 shows the comparison for a quiet, low beam power (2.4 MW), moderately low density (1.8×10^{13} cm^{-3}), L-mode plasma. The fast-ion distribution from TRANSP is input to the FIDA simulation code. The central range of the spectrum ($E < 20$ keV) is not simulated for two reasons. First, the measured spectrum over that range is contaminated by halo emissions, edge neutral emissions, and beam neutral emissions. Second, it is very inefficient to launch low energy fast ions in the simulation code. They have large populations compared to high energy fast ions. Moreover, they move slowly, which means more time steps for them when solving the collisional-radiative equations.

For the channel with a major radius of 180 cm, the simulated spectrum is scaled by 0.75 in the figure. For the channel at 195 cm, there is no scaling and the agreement is believed to be fortuitous. Comparisons for other shots also reveal that the magnitudes are generally within 20%–30%, which is reasonable provided uncertainties in background subtraction, intensity calibration, and uncertainties in the simulated spectra associated with uncertainties in the plasma parameters and the calculated distribution function. The results of an extensive study of sensitivity of the FIDA simulation code (includ-

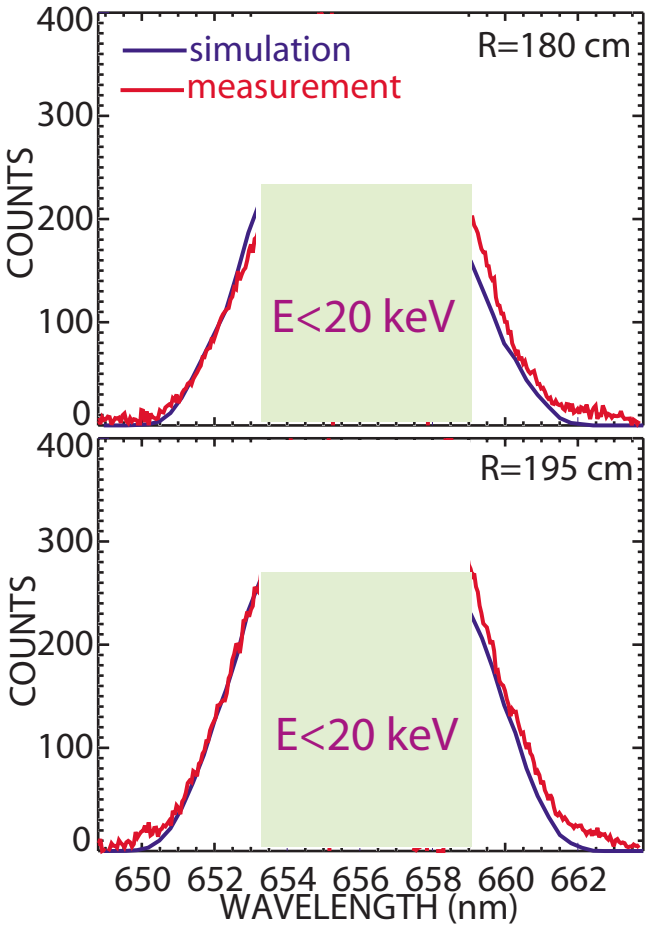

FIG. 3. (Color online) Comparison of the measured spectra and simulated spectra. There are no detectable instabilities at the time (1380 ms) of comparison (P_B=2.4 MW, B_T=2.0 T, I_p=1.0 MA, and single-null configuration). Error bars associated with random errors are less than the size of symbols (not shown).

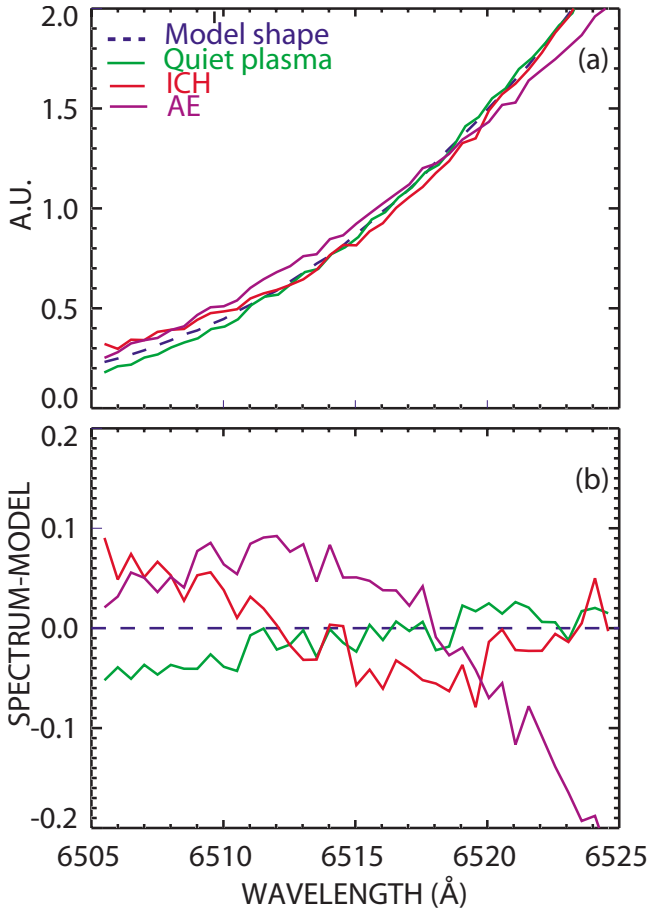

FIG. 4. (Color online) (a) Comparison of spectral shape in different plasma conditions. The quiet plasma case is from discharge 122073 at 2000 ms, the ICH case is from discharge 123117 at 2450 ms, and the AE case is from discharge 122527 at 2405 ms. The typical ("model") shape is the average of eight spectra with left beams in quiet plasmas. (b) The differences between the spectral shape of the three individual cases and the model shape.

ing TRANSP) on various plasma profiles are presented in the Appendix. Among the plasma parameters, electron density has the greatest effect on the FIDA spectrum. Estimates based on this study suggest that the uncertainty in the simulated intensity in Fig. 3 is ~20%.

For both chords, the spectral shape is in excellent agreement with theory. The simulated spectral shape depends on the fast-ion velocity distribution model and atomic rates. The shape agreements confirm that TRANSP models the fast-ion velocity distribution correctly and validate the atomic cross sections in the simulation code. Some minor discrepancies are readily explained. On the two ends, the small bumps are from imperfect removal of impurity lines. In the left range of the red side, there are huge carbon lines and they usually are removed by beam-on and -off background subtraction. When the carbon emission changes slightly between beam-on and beam-off, the background subtraction results in an error. As shown in the Appendix, although simulated spectral magnitude is very sensitive on plasma profile uncertainties, the simulated spectral shape is less affected by plasma profile uncertainties. This is one of the reasons that there is better agreement on spectral shape than spectral magnitude.

The spectral shape is determined by the fast-ion velocity distribution. One interesting question is: Does the fast-ion velocity distribution ever change? In other words, does the spectral shape ever change? Figure 4 shows the spectral shape of a vertical chord at 195 cm for different plasmas. For this study, the cleanest portion of the spectrum with minimum contamination by impurity lines is chosen. The dashed blue line is the typical shape, which is the average of eight spectra with left beams in quiet plasmas. The green line is also from a quiet discharge; however, the electron temperature is only 1.1 keV, which is very low for DIII-D discharges. In this case, the low energy signal agrees with the typical shape and the high energy signal is weaker. This is because there is less pitch angle scattering due to low electron temperature and therefore less fast ions with high vertical energies. The red line is a case with ICH for conditions similar to those documented in Ref. 18. In this case with fourth harmonic heating, the high energy signal is elevated compared to the typical shape, and the higher the energy, the larger the discrepancy. This is because the fast ions are accelerated by a finite Larmor radius ($K_\perp \rho$) effect and the higher the energy, the stronger the acceleration. The line in violet is a case with Alfvén activities. This case shows the strongest distortion of the spectral shape. The low energy

signal decreases and the high energy signal increases compared to the typical shape. This is because fast ions are expelled from the core region and those fast ions have higher vertical energy since the electron temperature is higher in the core region. Normally, fast-ion transport due to Alfvén activities can be observed by fast-ion spatial profile change. The shape study implies another way to see evidence of fast-ion redistribution through spectral shape change.

Spectral shape variation is also studied via the database. For each entry in the database, the spectral shape is compared to the model shape and the reduced chi-square is archived. The average of the reduced chi-square for quiet discharges is 0.33. Apparently we overestimated the experimental error associated with photon statistics and readout noise, resulting in reduced chi-square values much less than 1. Nonetheless, this comparison does show that the average reduced chi-square for discharges with ICH or strong AE activity is considerably larger: 0.44 and 0.50, respectively. Thus, it is evident that ICH and AE activity can alter the spectral shape.

IV. PARAMETRIC DEPENDENCIES AND CORROBORATIONS

In DIII-D, fast ions are born with an injection energy and pitch that is determined by the neutral beam injectors. In quiet plasmas, they slow down through coulomb collisions with thermal electrons and thermal ions. At the same time, they also experience pitch angle scattering through coulomb collisions with thermal ions. The fast-ion density is proportional to the fast-ion birth density and the slowing-down time. The fast-ion birth density depends on the deposition profile (which depends in a complex manner on the density profile) and the number of injected beam ions (which is proportional to the beam power P_{inj}). The slowing-down time on electrons is proportional to $T_e^{3/2}/n_e$, but collisions with thermal ions are also important, so the expected dependence is $f(T_e)/n_e$, where $f(T_e)$ is an increasing function of electron temperature. The fast-ion density scales approximately as

$$n_f \propto D(n_e)P_{\mathrm{inj}}f(T_e)/n_e, \tag{2}$$

where $D(n_e)$ is the beam deposition rate. In this section, we investigate the dependence of the FIDA signal on each of these parameters.

A. Injection energy

In a neutral-beam heated plasma without rf heating, the highest energy a fast ion can have is approximately the injection energy. Therefore, in the wavelength range above the injection energy, there should be little signal. This makes a very good first test of the FIDA diagnostic. In Fig. 5, the line in red is the FIDA spectrum for a discharge with an injection energy of 79 keV. On the two wings beyond the injection energy, the FIDA signal is virtually zero, as expected. Starting from the injection energy, the FIDA signal builds up gradually. This is because the FIDA vertical chord measures the vertical energy and the neutral beam injection angle includes a toroidal component. By the time fast ions are scattered to have a large pitch angle, most of them have slowed down considerably. To further check the injection energy dependence, a discharge with a different injection energy is compared. The line in blue is a discharge with an injection energy of 65 keV. It resembles the red line, except that the transition point moves from 79 keV to 65 keV, as expected.

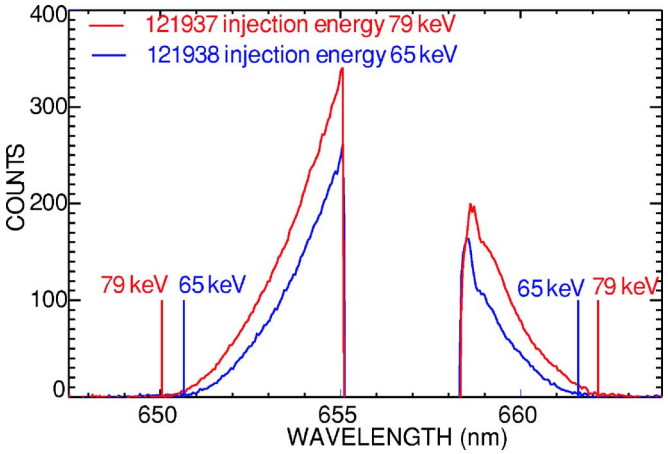

FIG. 5. (Color online) Spectra with different beam injection energies. The middle portion of the spectrum is blocked to avoid saturation due to bright interferences. The wavelengths corresponding to injection energies are labeled on both sides.

B. Injection angle

In DIII-D, neutral beams can be injected at two different angles. The radii of tangency for left beams and right beams are 1.15 and 0.76 m, respectively. Right beams are more perpendicular and therefore, they introduce fast ions with higher perpendicular energy. Since the FIDA vertical channels measure the vertical energy, over the high energy range, the FIDA signal should be stronger because there is less pitch angle scattering required. In Fig. 6, the discharge has left beams only in the early time and later it switches to right beams. Over the two phases, all the fast-ion relevant param-

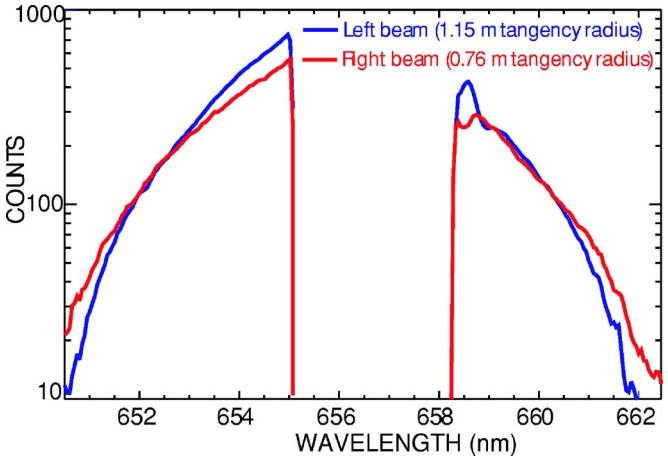

FIG. 6. (Color online) Spectra with different injection angles. For the more perpendicular right beam case, the 330 left beam is modulated in order to take the FIDA measurements with a left beam fraction of 0.2.

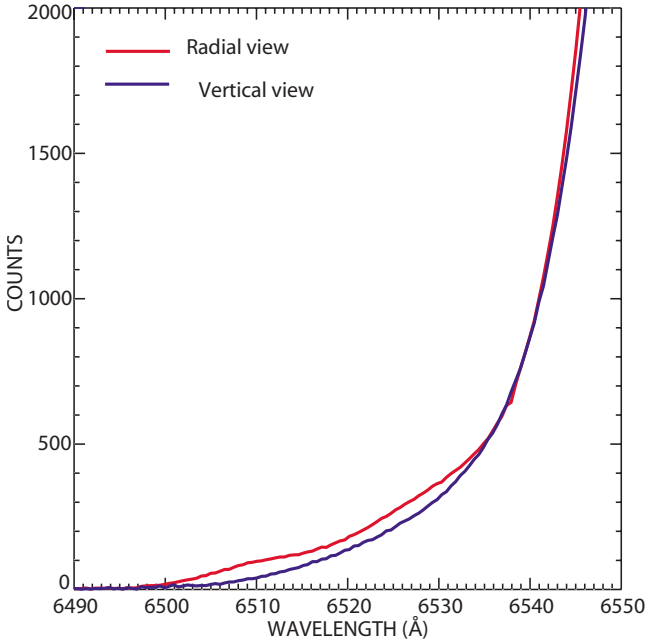

FIG. 7. (Color online) View comparison. The radial view is from discharge 122062 at 1670 ms and the vertical view is from discharge 122060 at 1670 ms. Both views are looking at 179 cm major radius. The two discharges have very similar plasma parameters.

eters are kept similar. In the high energy range, the FIDA signal is substantially elevated during right beam injection, as expected.

C. Viewing angle

In order to measure the full FIDA spectrum, a perpendicular view is required to minimize the Doppler shift of neutral beam emission. For a nonperpendicular view, one-half of the FIDA spectrum is clean with the other half contaminated by beam emission. It is interesting to compare which view has the stronger signal. In the current FIDA system, there is a radial chord viewing at the same major radius as one of the vertical views. Since the redshift side of the radial view spectrum is contaminated, only the blueshift side is compared (Fig. 7). The spectral shape comparison shows that the radial view detects relatively stronger signal over the high energy range. To explain the difference, a set of angles relevant to the views and fast ions are calculated. The initial fast-ion pitch angle at the chord location is 50.4°, the pitch angle of the radial view is 82.4°, and the pitch angle of the vertical view is 91.1°. For a fast ion to contribute to the high energy range in the spectrum, it needs to be scattered to be around the pitch angle of the viewing chord and at the same time, slowing down should be minimized. Therefore, when the pitch angle of the view is closer to the initial fast-ion pitch angle, fast ions are more likely to be scattered without being significantly slowed down. In the above comparison, the radial view is closer to the initial fast-ion pitch angle resulting in stronger signal over the high energy range. The numbers of the angles show that the present views are far from optimized. To maximize the signal in future implementations, views should be chosen to be as close to the initial fast-ion pitch angle as possible. This usually results in beam emission contamination on the blue side, which is more favorable for the FIDA diagnostic. However, when there are both co- and counter-neutral beams, views on the counter-neutral beam can be optimized to measure circulating fast ions produced by co-beam injection.

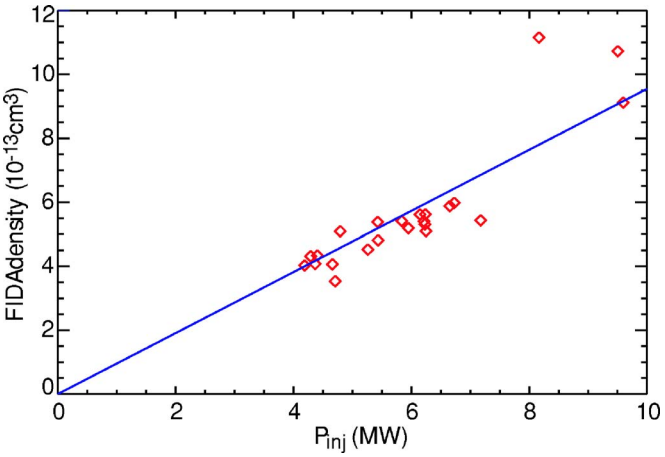

FIG. 8. (Color online) Beam power dependence of the FIDA signal. The FIDA signal is averaged over E_λ between 50 keV and 60 keV. The line is a linear fit of the data through the origin.

D. Injection power

Equation (2) shows that, provided that the electron density and electron temperature are fixed, the fast-ion density is proportional to beam power. On the other hand, provided that there is minimal velocity distribution change, the fast-ion density is also proportional to the FIDA density. Therefore, a linear relationship between the FIDA density and the beam power is expected when the relevant parameters are similar. This correlation is studied in the database (Fig. 8). In this study, electron density on the magnetic axis is held to be between 4.1×10^{13} and 5.0×10^{13} cm^{-3}. The density profiles are very similar and therefore the deposition profiles should have minimal differences. Electron temperature on the magnetic is held to be between 2.9 and 3.5 keV. The relatively broad ranges are necessary to get more data points from the database. The correlation coefficient is 0.89. The scatter is likely caused by the finite ranges in electron temperature and electron density and uncertainties in the beam neutral calculation.

E. Electron temperature and corroborations

The fast-ion slowing-down time is an increasing function of electron temperature. As a result, the fast-ion density is an increasing function of electron temperature. Moreover, the relative importance of pitch angle scattering increases with electron temperature and consequently the number of fast ions with higher perpendicular energy increases. To study the FIDA electron temperature dependence, electron cyclotron heating is modulated to vary the electron temperature. Figure 9 confirms that the FIDA signal goes up and down with electron temperature with a delay, which is caused by the finite slowing-down time. The slowing-down time for full energy beam ions on axis is estimated to be

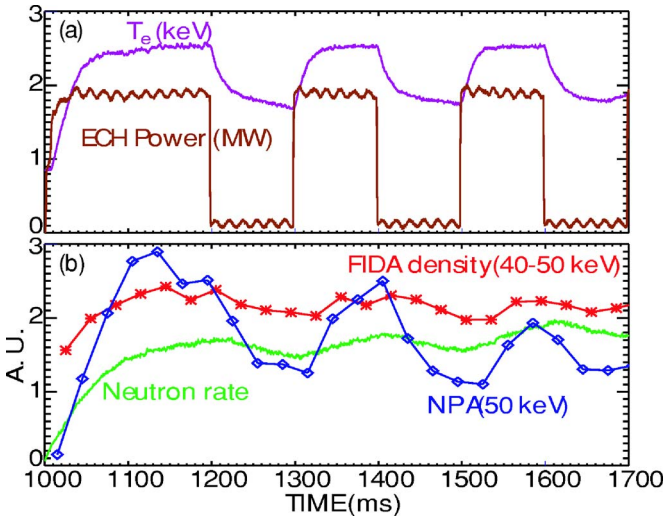

FIG. 9. (Color online) (a) Time evolution of ECH power and electron temperature. (b) Time evolution of FIDA density, NPA signal, and neutron rate.

110–150 ms. The FIDA signal is not as sensitive as the NPA. The fundamental reason is that the NPA only measures a point in velocity space, while FIDA measures a collection of fast ions in velocity space, so pitch angle scattering has a much bigger effect on the NPA. The neutron diagnostic is also a velocity space integrated diagnostic, and not surprisingly, like FIDA, it changes with electron temperature in a more gradual way.

The electron temperature dependence is also studied in the database. To single out the electron temperature effect, all the other relevant parameters are kept similar, including electron density, beam power, and left beam fraction. The vertical axis is chosen to be FIDA density to get rid of the neutral density factor on FIDA. Figure 10 shows that the FIDA signal increases with electron temperature in the database. The scattered points are caused by loose constraints on the other parameters due to limited database entries.

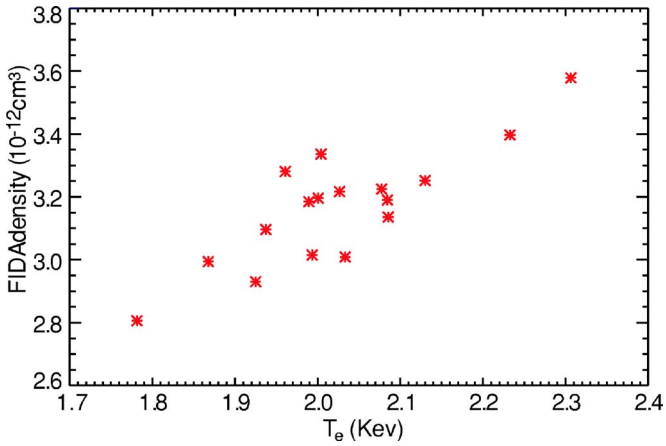

FIG. 10. (Color online) Electron temperature dependence of the FIDA density in the database. The FIDA signal is averaged over E_λ between 40 and 60 keV. Electron density is held to be between $(2.5–3.5)\times 10^{13}/\mathrm{cm}^3$.

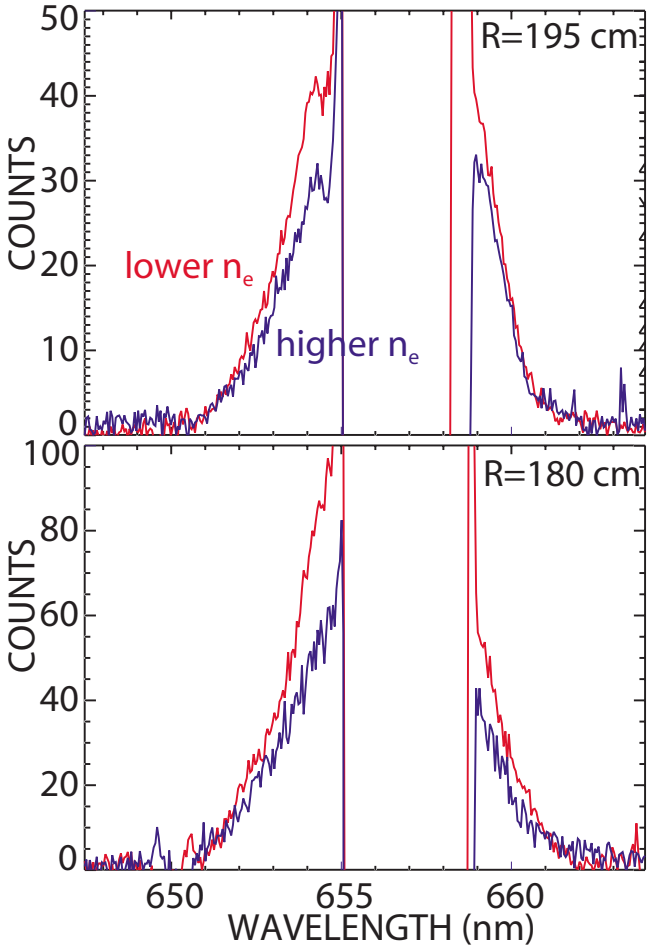

FIG. 11. (Color online) Electron density dependence of the FIDA signal. The spectrum with lower electron density is at 1930 ms with an electron density of $3.8\times 10^{13}/\mathrm{cm}^3$. The spectrum with higher electron density is at 2750 ms with an electron density of $5.0\times 10^{13}/\mathrm{cm}^3$.

F. Electron density dependence

Electron density affects the FIDA signal in two ways: first, fast-ion density decreases with increasing electron density due to changes in beam deposition and slowing-down time; second, the injected neutral density decreases with electron density because of the increased stopping power. Figure 11 shows the electron density dependence in a particular discharge. This discharge has different densities at the two times with all the other relevant parameters similar. For both chords, the FIDA signal drops considerably during the high density phase. The chord at 195 cm shows less drop because the electron temperature is 15% higher at the later time, which offsets some of the dip.

To study the electron density dependence quantitatively, a discharge with a period during which the electron density steadily ramps up is selected. The points in red in Fig. 12 are the FIDA measurements and, as expected, they decrease with increasing electron density. To calculate the expected dependence, a simple model is built for the FIDA signal. The model is the product of total neutral density, the deposition rate of the full energy component, and the slowing-down time. Note that the product of the last two terms is proportional to fast-ion density. Only the deposition rate of the full

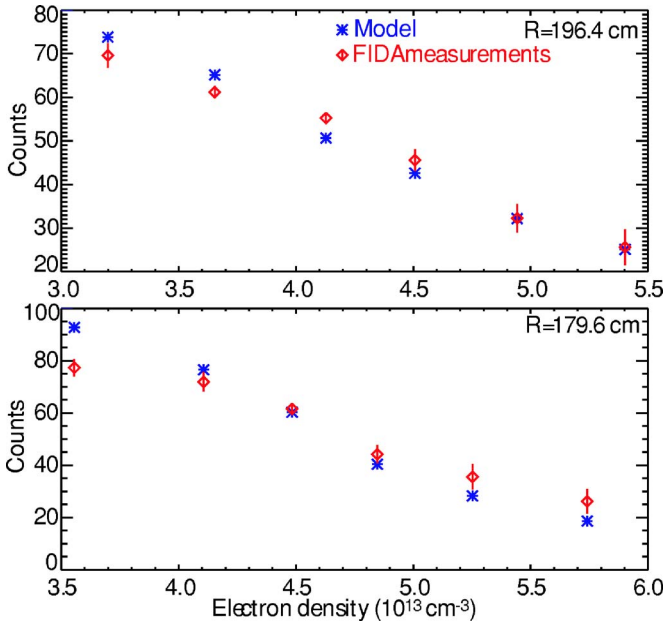

FIG. 12. (Color online) Electron density dependence of the FIDA signal and comparison with the simple model described in the text. Each FIDA data point is averaged over E_λ between 25 and 60 keV and a 200 ms time window.

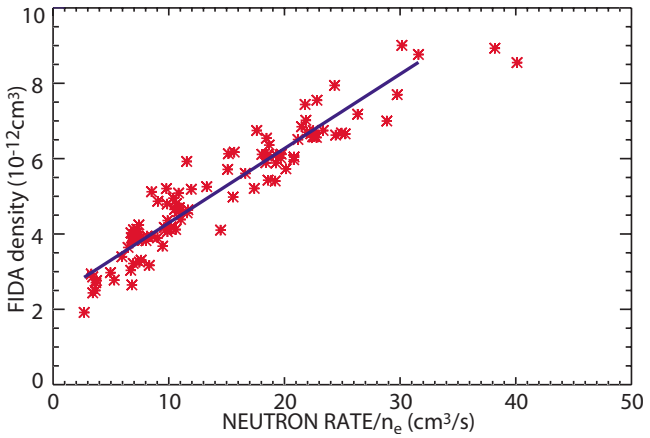

FIG. 13. (Color online) Correlation between the FIDA diagnostic and the neutron diagnostic. The FIDA signal is averaged over E_λ between 30 and 80 keV from a chord viewing 195 cm major radius. The solid line is a linear fit.

energy component is adopted because the FIDA measurements are the high energy signal, which exceeds the half and one-third energy components. All atomic physics is neglected in this model, which is legitimate when the velocity distribution does not change and only the signal level is concerned. With one free parameter (constant scaling), the model shows very good agreement with the measurements on both chords.

G. Neutron corroboration

The neutron diagnostic is another fast-ion diagnostic and the correlation between FIDA and the neutron diagnostic is investigated in the database. As usual, the vertical axis is FIDA density, which is proportional to fast-ion density. In most discharges in this study, beam-thermal reactions dominate the neutron production and therefore, the neutron rate over electron density is approximately proportional to the fast-ion density. As shown in Fig. 13, a strong correlation is observed between FIDA and the neutron diagnostic. The fitted line does not go through the origin because for low values of n_e, beam-beam reactions constitute ~25% of the total neutron rate, so neutron rate/n_e overestimates the fast-ion density.

V. SPATIAL PROFILES

As shown in Fig. 2, there are nine vertical chords available for the FIDA measurements, which allow us to obtain the fast-ion spatial profiles. However, the chords are different in many aspects. There are two systems, the dedicated system and the Reticon system, which have different components and detectors. Even within a system, the spot sizes, the solid angles subtended by the collection lens and the light paths differ substantially. There are two ways to overcome the chord difference. One is to use the relative FIDA profile, and the other is to take the absolute FIDA profile with all the chord specifics removed.

To generate a FIDA profile, an energy window is chosen first. For each chord, the signal is then averaged over the selected energy window. A relative FIDA spatial profile is a profile obtained by dividing one raw profile by another raw profile for different plasma parameters. Since the relative profile only provides relative information, it is independent of chord specifics and requires no special processing for individual chords. Figure 14 shows a typical relative profile in a quiet plasma. Two time slices (at 2285 and 2700 ms) are chosen with a substantial density change [Fig. 14(a)]. In quiet plasmas, the fast-ion density is inversely proportional to the electron density. Therefore, the fast-ion density at the later time is expected to be higher. This is confirmed by the beam pressure profile calculated by TRANSP [Fig. 14(b)]; the shapes of the predicted beam-ion density profiles are similar. An independent measurement of the beam pressure profile is available from EFIT[19] equilibrium reconstructions that rely on motional Stark effect polarimetry,[20] magnetics, and T_e isotherm measurements. The thermal pressure profile from kinetic measurements is subtracted from the EFIT pressure profile to obtain the beam-ion pressure.[21] For the conditions of Fig. 14, the absolute uncertainty in the fast-ion profiles are ~20% and the relative uncertainties are about ~10%. The profiles obtained in this fashion are consistent with the TRANSP predictions within these uncertainties and confirm that the fast-ion behavior is close to classical in this discharge. TRANSP runs with various spatially uniform *ad hoc* beam-ion diffusion coefficients are compared with the EFIT beam pressure profile. Error bars imply that diffusion coefficient must be within 0.1 m^2/s. The FIDA profile is compared with the prediction of the simulation code in Fig. 14(c). The FIDA signal is proportional to both the fast-ion density and the neutral density. Since the fast-ion density peaks on axis, but the neutral density is largest at the edge, the simulated profiles peak between the magnetic axis and the edge. At 2700 ms with lower electron density, the simulated FIDA

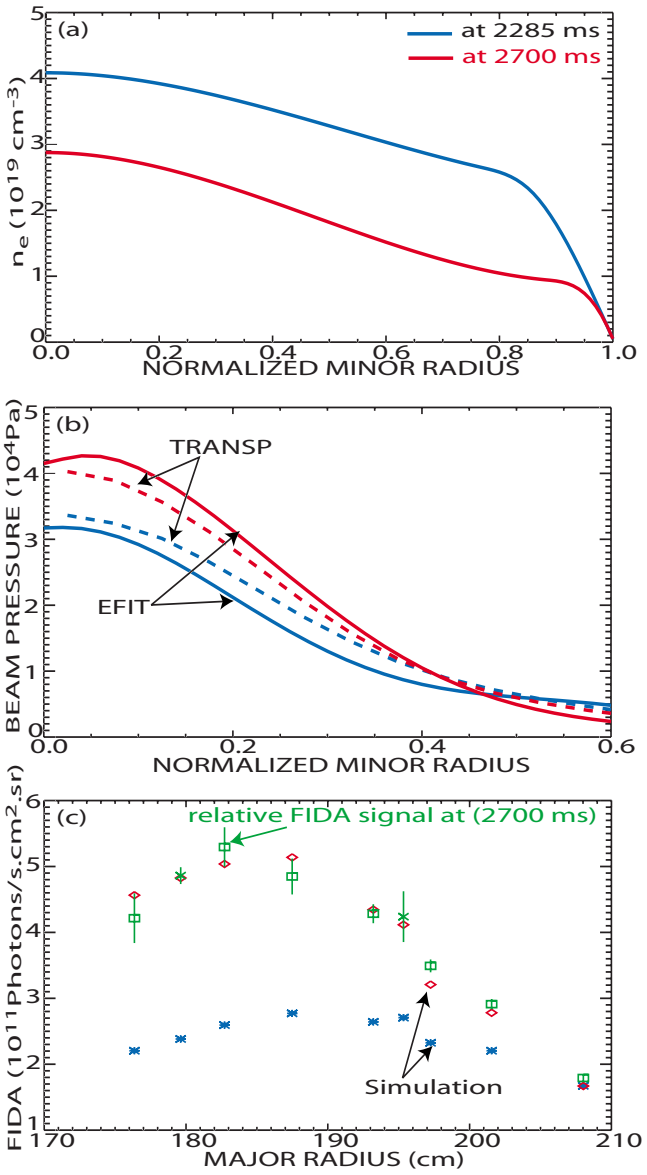

FIG. 14. (Color online) (a) Electron density profiles vs normalized minor radius at 2285 and 2700 ms. (b) Beam pressure profiles from TRANSP (dashed) and EFIT (solid) versus normalized minor radius at the two times. (c) Simulated profiles and relative FIDA profile. The FIDA signal is averaged over E_λ between 20 and 40 keV.

profile is significantly elevated. The jump is more pronounced than that for beam pressure. This is due to the increased neutral density resulting from the lower electron density. To obtain the relative FIDA profile, the FIDA measurements at 2285 ms are scaled to match the simulated profile at 2285 ms and at 2700 ms, the FIDA measurements are scaled by the same factor. Excellent agreement is reached between the measured FIDA relative profile and the simulated profile. The error bars in the figure only address the random errors. In this quiet discharge, the systematic errors should be small. The agreement shows that FIDA relative profiles can provide precise information on how fast-ion profiles evolve.

The absolute FIDA profile is very challenging. To produce an absolute FIDA profile from the measurements, intensity calibration data for each chord are utilized to convert the

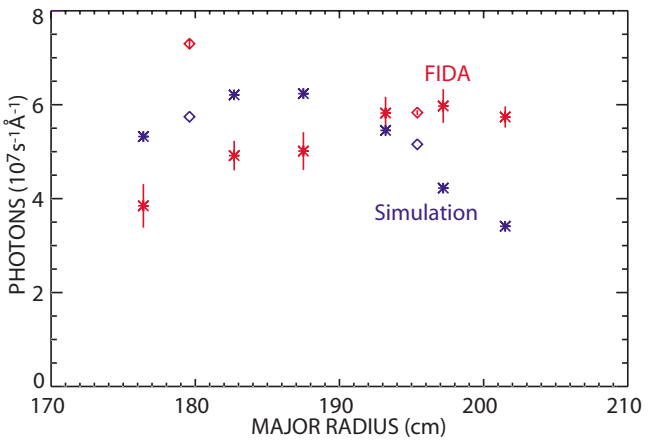

FIG. 15. (Color online) Absolute comparison of the measured FIDA profile and the simulated profile. The time of the comparison is at 2100 ms. The FIDA signal is averaged over E_λ between 30 and 60 keV. The CCD channels are shown in diamonds.

number of digitizer counts into numbers of photons. The chord specifics such as solid angles and spot sizes are normalized out. Figure 15 shows the comparison between the measured absolute FIDA profile and the simulated absolute FIDA profile in a quiet plasma. The magnitudes are within 30% for all the chords, which is very reasonable provided the uncertainties in data processing, plasma profiles input to the simulation code and intensity calibrations. The simulated profile shape is as expected, peaking at a point somewhere between the magnetic axis and the edge. However, the measured profile shape does not agree with the simulation. The difference between the CCD channels and the Reticon channels suggests that the intensity calibration is problematic. The errors are estimated based on the FIDA data only, without taking into account the uncertainties in intensity calibration. The modest error bars show that future prospect for absolute profiles is good with careful intensity calibration.

VI. CONCLUSION

FIDA measurements in quiet plasmas are compared with simulations that use the fast-ion distribution from TRANSP. The spectral shape is in excellent agreement, indicating that the Coulomb collision model in TRANSP is valid and the atomic cross sections in the FIDA simulation code are accurate. The absolute signal magnitude is within 30%, resulting from a variety of uncertainty sources. A sensitivity study suggests that the uncertainty of electron density profile is the most influential one and could account for a large portion of the discrepancy.

The parametric dependencies of the FIDA diagnostic in quiet plasmas are studied extensively both in individual discharges and in a large database. All of the dependencies are as classically expected, suggesting that the FIDA diagnostic is well understood. The NPA and neutron diagnostics corroborate the FIDA diagnostic.

A set of vertical chords allows us to obtain the FIDA spatial profile. The relative profile is compared with the simulated profile and shows excellent agreement. Error bars imply that fast-ion diffusion coefficient must be within

0.1 m^2/s. However, obtaining the absolute profile is problematic currently, but may be resolved in the future with a careful intensity calibration.

The successful benchmarking of FIDA measurements in these quiet plasma establishes the reliability of this diagnostic technique, allowing its confident application in more complicated situations. In one recent study, the FIDA diagnostic measured distortions of the fast-ion energy spectrum during ICH and determined the radial location of the acceleration.[6] In another, flattening of the fast-ion profile by strong Alfvén activity was observed.[22] FIDA spectroscopy is now established as a powerful diagnostic of the fast-ion distribution function.

ACKNOWLEDGMENTS

The assistance of R. Boivin, M. Wade, E. Strait, C. Petty, N. Brooks, D. Kaplan, P. Gohil, J. Lohr, H. Chiu, and the entire DIII-D team is gratefully acknowledged.

This work was supported by the U. S. Department of Energy Subcontract No. SC-G903402, and Contract Nos. DE-FC02-04ER54698 and DE-AC02-76CH03073.

APPENDIX: SENSITIVITY TO PLASMA UNCERTAINTIES

Plasma profile uncertainties influence the calculated FIDA signals via three distinct physical mechanisms. One mechanism affects the atomic radiative-collisonal calculations, a second mechanism affects the calculations of the neutral density, and a third modifies the beam-ion distribution function. The signal strength is proportional to both the neutral density and the beam-ion density.

To assess the influence of these uncertainties on the calculated FIDA spectra at various radial locations, a systematic modeling study has been undertaken. We analyzed a typical DIII-D L-mode plasma (#122060 at 2.05 s) heated with two 80 keV beams, and modulated power between 2.5 and 5.0 MW. The central plasma density and temperature at the time of interest were $n_e(0)=4.0\times10^{13}$ cm^{-3} and $T_e(0)=3.0$ keV. Individual plasma profiles, such as electron density and temperature, ion temperature and Z_{eff}, were scaled up and down by 20% across the entire plasma column and the calculated spectra were compared with the baseline spectra, where unmodified experimental profiles were used.

Monte Carlo simulations with 10^7 particles were necessary to obtain satisfactory spectra. Identical random seed was used in all simulations to eliminate the effect of the MC noise. Separate simulations with arbitrary seed numbers had shown that this noise level is about ±2% for a 10^7 particle simulation. The MC statistics are much worse for particles with energies above 70 keV because too few beam ions have such high vertical energy. It takes about 30 h on a 3 GHz Intel® Xenon processor to calculate the spectra at ten radial locations.

Since FIDA signals typically vary over three orders of magnitude in the spectral range of interest, it is necessary to calculate ratios of signals from simulations with modified plasma profiles to those with the baseline profiles.

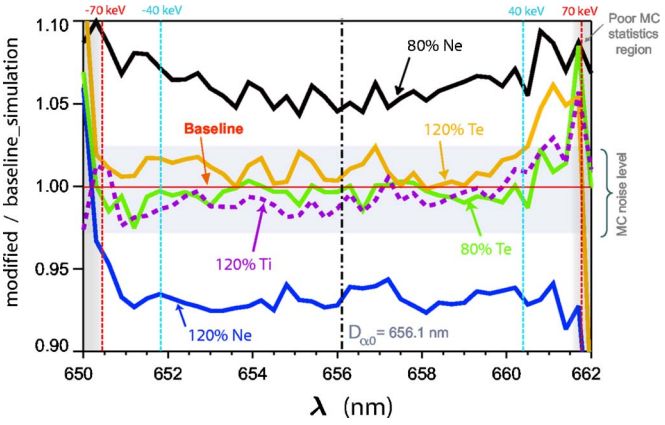

FIG. 16. (Color online) Changes in the calculated FIDA signal at $R=180$ cm caused by changes in neutral density associated with variations in plasma parameters.

We focus now on the modeling results for a vertical channel 4 cm away from the plasma center ($R_0=176$ cm)—the effect on channels further away is smaller. It was found that T_e and T_i plasma profile variations affect the atomic radiative-collisonal calculations close to the MC noise level, and thus can be ignored. The influence of the electron and ion temperature variations on the calculated FIDA spectra via the effect on the calculated neutrals is similar; however, the electron density variation has about three times larger influence and cannot be ignored (Fig. 16). Note that in all these simulations the beam-ion distribution function from the baseline TRANSP model was used.

Higher electron density lowers the injected neutral density by increasing the electron impact ionization of neutrals; higher ion density increases charge exchange with thermal ions. For a given beam-ion distribution function, the smaller neutral density leads to weaker FIDA signals, as seen in Fig. 16, where 20% increase in the electron density is responsible for a ~7% reduction of the calculated FIDA signal due to the impact on neutrals alone.

FIDA diagnostics are designed for indirect measurement of the beam-ion distribution function f_B; thus, useful FIDA

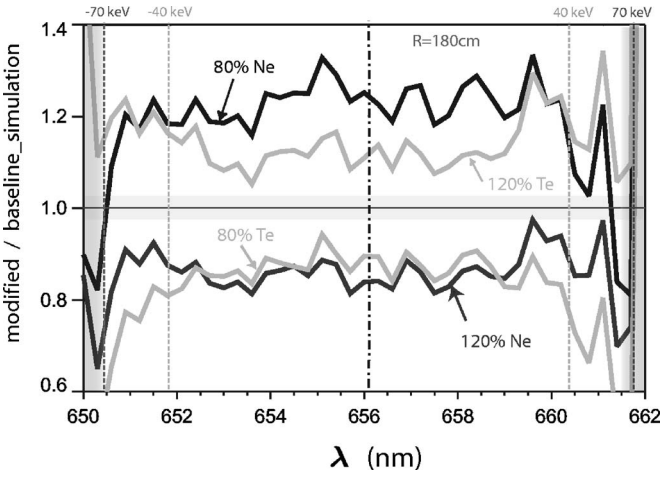

FIG. 17. FIDA signals are sensitive to modifications of the beam-ion distribution function due to plasma profile uncertainties.

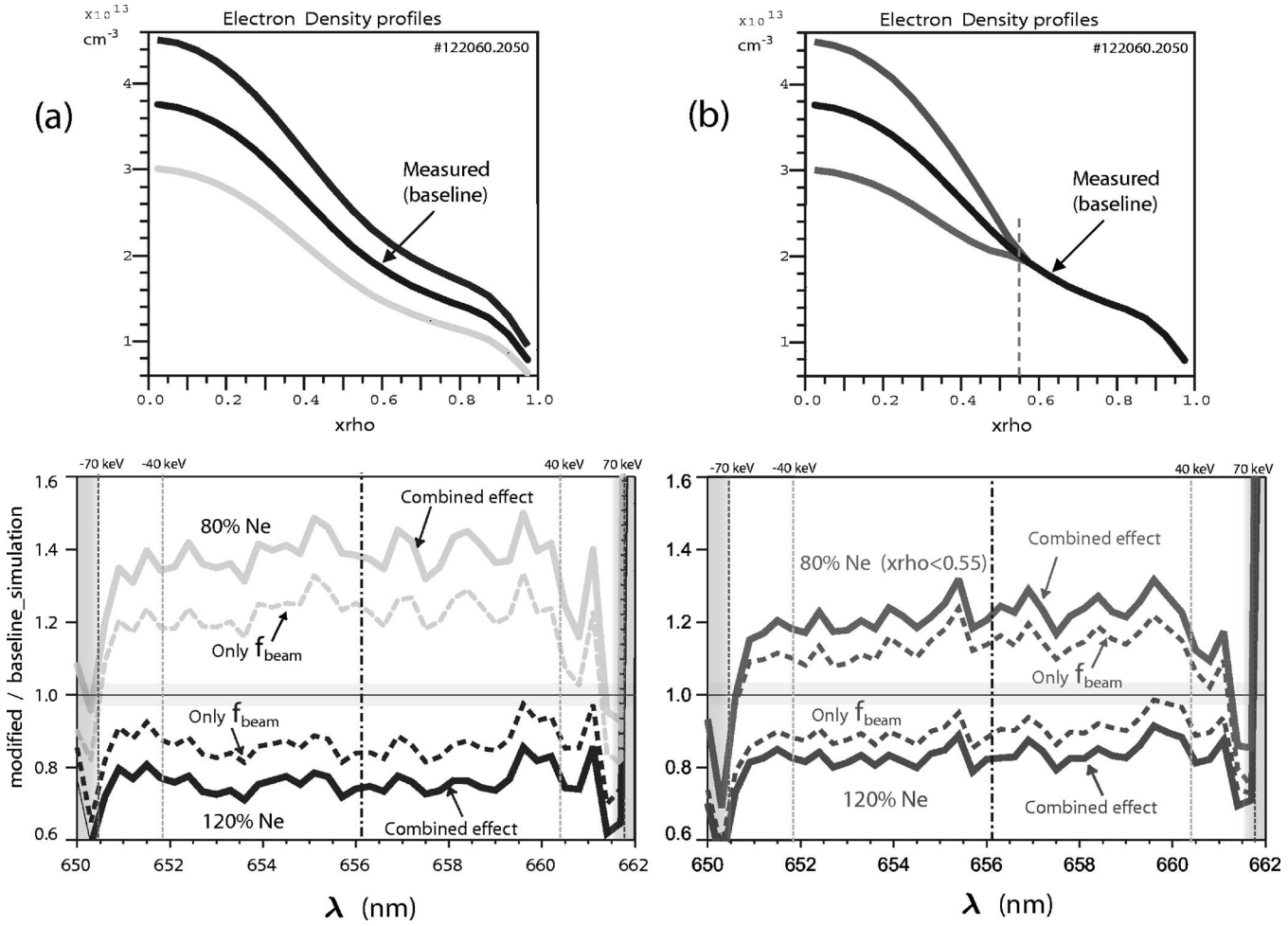

FIG. 18. FIDA signal sensitivity due to combined effect of electron density on neutrals and fast-ion distribution: (a) uniformly scaled profile and (b) profile scaled in the inner plasma half.

spectra require sensitivity to f_B variations. Energetic ions in DIII-D plasmas slow down on both electrons and thermal ions. The corresponding beam-ion slowing-down time on electrons in the absence of MHD activity is

$$\tau_{\mathrm{sl},e} \sim T_e^{3/2}/n_e. \tag{A1}$$

Lower electron temperature or higher density lead to shorter slowing-down times and lower beam-ion densities; i.e., weaker FIDA signals. The opposite is true for higher temperatures and lower densities. These conclusions are corroborated with Fig. 17, where modeling results from FIDA simulations with modified beam-ion distribution functions are shown. These functions were obtained from TRANSP simulations where a single plasma profile was uniformly scaled up or down by 20%. To provide sufficiently smooth beam-distribution functions, all TRANSP runs in this study used 100 000 beam-ion particles.

Impurity density variations are also expected to affect the beam-ion distribution function. We studied this effect by scaling Z_{eff} in TRANSP by ±20%. Higher Z_{eff} implies stronger pitch angle scattering of the beam ions into the higher energy range (>30 keV). The expected increase in the FIDA signal strength for $E>30$ keV was indeed observed, and was in the 5%–10% range.

Figures 16 and 17 show that the electron density uncertainty has a compounding effect on the calculated FIDA signals: n_e variations alter the spectra due to the change in neutral density and the beam distribution function in the same

TABLE I. FIDA signal response to uniformly 20% increase of various plasma parameters.

Parameters	Atomic rates		Neutrals		Fast ions		Total effects	
	Inner chord	Outer chord	Inner chord	Outer chord	Inner chord	Outer chord	Inner chord	Outer chord
$n_{e(+20\%)}$	⋯	⋯	−7%	+3%	−17%	−14%	−24%	−12%
$T_{e(+20\%)}$	0%	0%	1%	0%	+11%	+17%	⋯	⋯
$T_{i(+20\%)}$	−2%	−2%	−1%	−3%	⋯	⋯	⋯	⋯

direction. Another important question is how profile changes in the inner half of the plasma column alter the calculated spectra. In DIII-D, fitting of the measured electron densities with the Thomson scattering diagnostics introduces the largest uncertainties in the plasma center. Modeling results addressing these questions are shown in Fig. 18. By lowering n_e everywhere by 20%, the FIDA signal at $R=180$ cm increases by ~35%. n_e lowered by 20%, just in the inner plasma half, increases the signal by ~20%. The n_e increase has somewhat smaller effect: ~25% and ~20% signal decrease, respectively. Density variations influence the outer channels less, and the influence for the most peripheral channels ($R\sim 210$ cm) decreases to about half (<20%) of that for the central channels (not shown).

The sensitivity study results are summarized in Table I. The plasma parameters are uniformly increased by 20% and the resultant changes of the FIDA signals are listed. Since the effect varies across the radial location of the chords, two representative chords are chosen with the inner chord at 180 cm and the outer chord at 212 cm. The effect on other chords can be estimated based on their chord locations. The dashed cells mean that the study has not been done yet. Mostly, it is because the expected effect is trivial or could be inferred. Note that the effect on Z_{eff} is not listed. The resultant spectrum is not uniformly affected, and for some reason, the spectral ratio is very noisy.

Our choice of varying plasma parameters by 20% was motivated by the desire to observe clear trends and produce easily distinguishable results. As expected, the uncertainty in the electron density profile affects the calculated FIDA spectrum the most. In reality, for DIII-D this uncertainty is about 10%, so the ultimate uncertainty for all calculated spectra should be in the 15%–20% range.

[1] M. Shimada, D. J. Campbell, V. Mukhovatov *et al.*, Nucl. Fusion **47**, S1 (2007).
[2] W. W. Heidbrink and G. J. Sadler, Nucl. Fusion **34**, 535 (1994).
[3] K.-L. Wong, Plasma Phys. Controlled Fusion **41**, R1 (1999).
[4] W. W. Heidbrink, K. H. Burrell, Y. Luo, N. A. Pablant, and E. Ruskov, Plasma Phys. Controlled Fusion **46**, 1855 (2004).
[5] Y. Luo, W. W. Heidbrink, K. H. Burrell, D. H. Kaplan, and P. Gohil, Rev. Sci. Instrum. **78**, 033505 (2007).
[6] W. W. Heidbrink, Y. Luo, K. H. Burrell, R. W. Harvey, R. I. Pinsker, and E. Ruskov, Plasma Phys. Controlled Fusion **49**, 1457 (2007).
[7] G. Mckee, R. Fonck, B. Stratton *et al.*, Phys. Rev. Lett. **75**, 649 (1995).
[8] M. G. von Hellermann, W. G. F. Core, J. Frieling, L. D. Horton, R. W. T. Konig, W. Mandl, and H. P. Summers, Plasma Phys. Controlled Fusion **35**, 799 (1993).
[9] H. Bindslev, J. A. Hoekzema, J. Egedal, J. A. Fessey, T. P. Hughes, and J. S. Machuzak, Phys. Rev. Lett. **83**, 3206 (1999).
[10] Y. Luo, W. W. Heidbrink, and K. H. Burrell, Rev. Sci. Instrum. **75**, 3468 (2004).
[11] T. N. Carlstrom, G. L. Campbell, J. C. DeBoo *et al.*, Rev. Sci. Instrum. **63**, 4901 (1992).
[12] T. N. Carlstrom, D. R. Ahlgren, and J. Crosbie, Rev. Sci. Instrum. **59**, 1063 (1998).
[13] M. E. Austin and J. Lohr, Rev. Sci. Instrum. **74**, 1457 (2003).
[14] R. Philipona, E. J. Doyle, N. C. Luhmann, W. A. Peebles, C. Rettig, K. H. Burrell, R. J. Groebner, H. Matsumoto, and the DIII-D group, Rev. Sci. Instrum. **61**, 3007 (1990).
[15] W. W. Heidbrink, P. L. Taylor, and J. A. Phillips, Rev. Sci. Instrum. **68**, 536 (1997).
[16] W. W. Heidbrink, Rev. Sci. Instrum. **59**, 1679 (1988).
[17] J. Egedal and H. Bindslev, Phys. Plasmas **11**, 2191 (2004).
[18] W. W. Heidbrink, E. Fredrickson, T. K. Mau, C. C. Petty, R. I. Pinsker, M. Porkolab, and B. W. Rice, Nucl. Fusion **39**, 1369 (1999).
[19] L. L. Lao, H. St. John, R. D. Stambaugh, A. G. Kellman, and W. Pfeiffer, Nucl. Fusion **25**, 1611 (1985).
[20] B. W. Rice, D. G. Nilson, and D. Wroblewski, Rev. Sci. Instrum. **66**, 373 (1995).
[21] C. C. Petty, C. B. Forest, R. I. Pinsker, J. S. DeGrassie, F. W. Baity *et al.*, *Proceedings of 12th International Conference on Radio Frequency Power in Plasmas, Savannah, 1997* (AIP, Melville, NY, 1997), p. 225.
[22] W. W. Heidbrink, N. N. Gorelenkov, Y. Luo *et al.*, "Anomalous flattening of the fast-ion profile during Alfven eigenmode activity," Phys Rev. Lett (in press).